Elongation enhances migration through hydrodynamic shear

R. N. Bearon*
Department of Mathematical Sciences, University of Liverpool, Liverpool, L69 7ZL, UK

W. M. Durham
Department of Physics and Astronomy, University of Sheffield, Sheffield, S3 7RH, UK
(Dated: December 2, 2022)

Many species of plankton migrate through the water column to avoid predation and acquire resources available only at depth. These vertical migrations, however, can be thwarted by flow which is ubiquitous in the ocean and acts to reorient the motility of swimming plankton in different directions. The torques exerted on an organism by hydrodynamic shear are a strong function of its shape - while spherical organisms only experience the overturning effect of vorticity, more elongated organisms experience additional torques that tend to align them in the direction of principal strain. Recent simulations of directed migration through turbulence indicate that organisms with larger aspect ratios are capable of faster vertical migration, however, the underlying physical processes are not well understood. Here, we use simple models of flow to study how elongation affects the capacity of a swimmer to vertically migrate through shear. We explore how the orientation of a migrating swimmer in simple shear depends both on its aspect ratio and non-dimensional stability, highlighting where a unique stable upwards equilibrium is globally attracting, and where particles can undergo periodic orbits. In addition, we identify that stable up and down equilbria can coexist when there is a non-zero vertical component of vorticity. We go on to investigate how elongation affects the transport and spatial distribution of a migrating swimmer in an inhomogeneous Kolmogorov shear flow. Our results show that a swimmer's shape can profoundly affect its mean field behaviour in flow and tendency to aggregate in regions of high shear. These findings reveal how flow can select for the elongated morphologies commonly found in marine plankton and may also provide new insights to rationally design microrobots to navigate ambient flows.

I. INTRODUCTION

The motion of small spheroidal particles in a simple shear was first described by Jeffery in 1922 [1] and remains a cornerstone of modern fluid dynamics. Particles undergo periodic rotation along one of a family of "Jeffery orbits" selected by the particle's aspect ratio and initial orientation. Jeffery's work has shed light on remarkably diverse phenomena, including how small colloidal particles alter a fluid's bulk viscosity [2], how turbulence can alter the sedimentation rate of elongated negatively buoyant particles [3], and how fluid shear can control the rate at which light is attenuated in the upper ocean by preferentially aligning elongated particles in the same direction [4]. In addition to describing the motion of passive particles, this theory has also been used to understand how flow affects the distribution and transport of planktonic organisms that actively swim. While fluid shear generally acts to reorient the motility of swimmers away from their intended direction of travel, the dynamics of this interaction crucially depends on the organism's morphology. In this way, Jeffery's equations may also shed light on evolutionary pressures that help select for the shape of swimming organisms, which range from nearly spherical to highly elongated needle-like morphologies, provided they are sufficiently small so that inertia is negligible.

Motility can confer planktonic organisms many advantages, but in many aquatic environments the chief utility of motility is to perform daily vertical migrations through the water column [5, 6]. Phytoplankton often spend daylight hours near the surface where light is plentiful and descend to deeper depths at night to where limiting nutrients are more abundant [7]. On the other hand, many zooplankton often exhibit vertical migrations with the reverse pattern to avoid well-lit waters during the day because they are often predated on by larger organisms that use visual cues to detect them [5, 6]. To orient their motility in the vertical direction plankton use a variety of different mechanisms, including the ability to actively sense the direction of gravity [8] or via passive mechanisms that rely on asymmetries in either the morphology or mass density of their bodies [9–11]. Regardless of the particular mechanism that plankton use to bias their motility, their intended movement can be disrupted by fluid shear. This is because the torques that act to keep a swimmer pointed in a preferred direction are opposed by the torques arising from hydrodynamic shear. When an organism's swimming direction is dictated by the competition between a stabilising torque, that acts to keep

* rbearon@liverpool.ac.uk

a cell pointed in a certain direction, and torques due to hydrodynamic shear it is said to be undergoing gyrotaxis. One of the main model organisms used to study gyrotaxis is the unicellular phytoplankton *Chlamydomonas augustae* which behave effectively as spheres and thus are only affected by vorticity [11]. However, many phytoplankton and zooplankton are highly elongated (Fig. 1) so their orientation is a function of both the vorticity and rate of strain tensor.

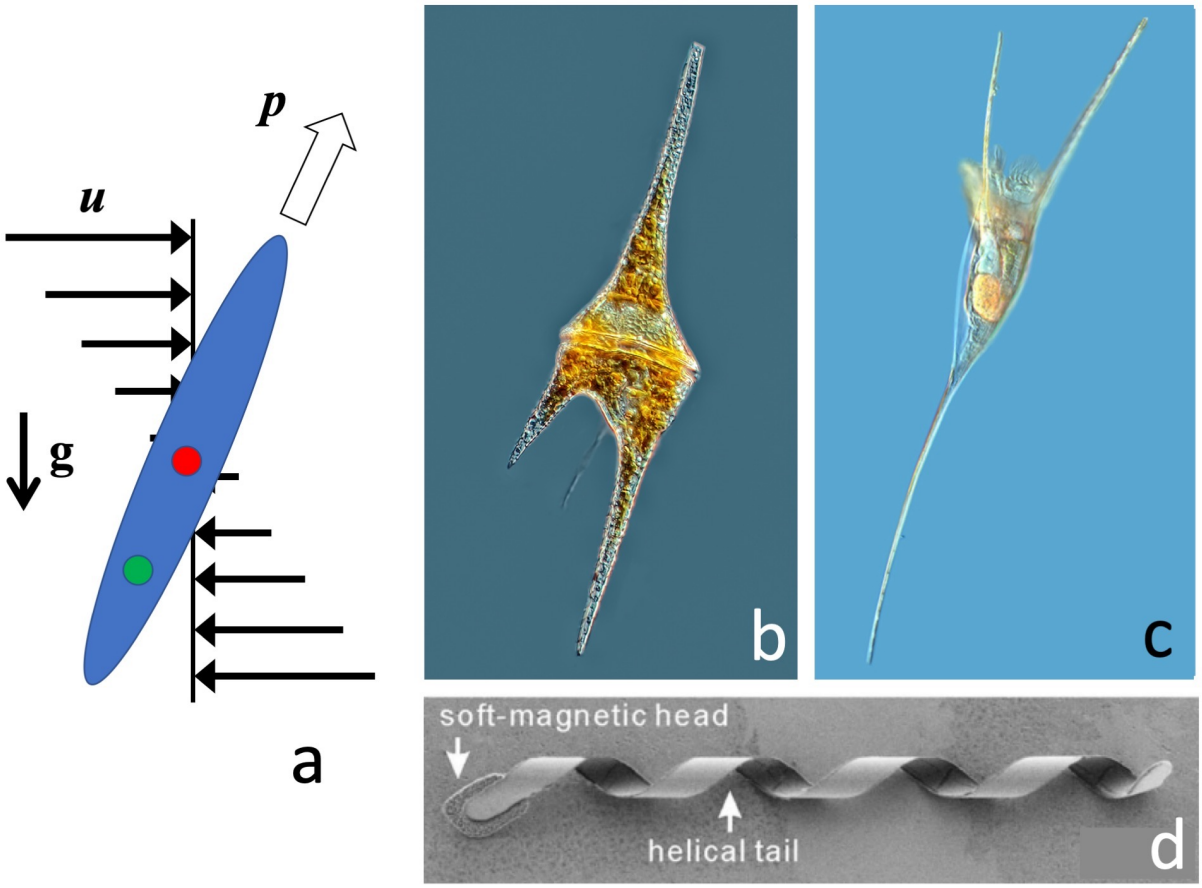

FIG. 1. Both motile planktonic organisms and engineered microswimmers can have highly elongated morphologies. (a) We idealise elongated swimmers as a prolate spheroid with aspect ratio n, whose centre of mass (green circle) is separated from their centre of buoyancy (red circle). This gives rise to a stabilising torque which tends to orient their swimming direction, $\mathbf{p}$, in a direction parallel to gravity, $\mathbf{g}$. However, flow (black arrows) also exerts a viscous torque that reorients swimming in other directions. (b,c) The toxic marine phytoplankton *Ceratium furca* and rotifer *Kellicottia longispina* both perform diel vertical migrations and possess long spines that dramatically increase their effective aspect ratio. *Ceratium furca* is approximately 100 µm long, while *Kellicottia longispina* is approximately 500 µm long. (d) An engineered microswimmer, inspired by bacteria, has a magnetic head that can be actuated to drive rotation about its long access for propulsion, as well to actively guide steering. This microswimmer is approximately 50 µm in length. Panel b was kindly provided by Rogelio Moreno (www.flickr.com/photos/rogeliomorenog), Panel c was kindly provided by Antonio Guillén (Proyecto Agua), and Panel d was reproduced with permission from [12].

The interplay between fluid flow and gyrotactic motility has been studied in a wide variety of different contexts. Pedley and Kessler [13], which we shall refer to as P&K, used a linear stability analysis to show that elongated swimmers could reach a stable equilibrium orientation in simple shear provided that the shear rate was below a critical value. Above this critical value, swimmers tend to tumble end over end. Almog and Frankel [14] analysed the orientation of non-motile dipolar particles in simple shear – identifying parameter regimes where the rotary motion converges to either a stable limit cycle or to an equilibrium orientation analogous to the one predicted by P&K and resolved how these depend on the particle's initial orientation.

Subsequent experiments and simulations have shown that vertical migration of unicellular phytoplankton can be fully suppressed in regions where the hydrodynamic shear is sufficiently high, resulting in the accumulation of cells in thin layer aggregations [15]. This mechanism – called "gyrotactic trapping" – was subsequently analysed theoretically using a dynamical systems approach that considered spherical cells swimming through a one-dimensional sinusoidal

Kolmogorov flow model [16, 17]. More complex patterns of aggregation have been observed when gyrotactic swimmers interact with analytical two and three dimensional flows, which have been shown to be strongly affected by elongated cell morphologies [18, 19].

Beyond analytical models of flow, gyrotactic motility has also been studied in the context of bioconvection, which occurs in highly concentrated cell suspensions, and turbulence, the disordered fluid motion found in the natural habitat of many gyrotactic organisms. Bioconvection occurs when cells, which are typically slightly more dense than the fluid in which they live, form local accumulations to produce density instabilities. Whether one considers the over-turning instability that occurs in shallow chambers, or the formation of plumes that occurs in deeper chambers, gyrotactic motility generates a positive feedback by redirecting the motility of cells so they accumulate in downwelling regions, which thereby increases the rate of downward flow [20]. While bioconvection occurs only in very dense suspensions, many gyrotactic organisms live in highly dynamic aquatic environments where ambient flows reorient the direction of swimming. Models of turbulence have shown that upwards swimming, spherical gyrotactic swimmers tend to accumulate in downwelling regions of homogeneous, isotropic turbulence, while more elongated swimmers instead tend to accumulate in upwelling regions [21, 22]. Moreover, elongated swimmers are able to keep more of their motility oriented in the vertical direction compared to spherical swimmers because they are stabilised against flow induced tumbling [21]. Both of these effects enhance the rate at which elongated swimmers can traverse a turbulent water column, however, the underlying physical mechanisms are not fully understood.

In this study, we develop a mathematical framework to understand how swimmers migrating in a particular direction respond to hydrodynamic shear. We initially focus our attention on 2D planar flows, with vorticity perpendicular to the restoring force, but allow swimmers, modelled as rigid spheroids, to move freely in 3D. We find that elongation enhances the ability of swimmers to migrate vertically through the water column, and explain the underlying mechanisms in detail. Specifically, we present the orientation dynamics of swimmers located in horizontal and vertical shear flow as a function of shape and a non-dimensional stability parameter. We identify the nature of the equilibria, and constraints on the parameters and initial conditions for these equilibria to be feasible, stable, and globally attracting. We illustrate how these effects can affect migration through inhomogeneous flow conditions using a sinusoidally varying Kolmogorov flow, where we demonstrate how elongation enhances the ability of swimmers to migrate vertically, and how tumbling-induced thin layers in horizontal flow vary with cell shape. Finally we demonstrate the robustness of our results; first through considering the effects of rotational diffusion, and then through extension of our analysis to weakly 3D flows, where we modify the simple shear flow to allow for a non-zero component of vertical vorticity.

II. MODEL

We consider the deterministic motion of an axisymmetric particle with symmetry axis given by the unit vector $\mathbf{p}$. We suppose the rotation of the particle is determined as a function of the non-dimensional vorticity $\boldsymbol{\omega}$ and rate of strain tensor $\mathbf{E}$ of the flow field, and the stability number, Ψ, which represents the timescale for a particle to reorientate to its preferred direction, $\mathbf{k}$, non-dimensionalised by the characteristic shear rate:

$$\frac{d\mathbf{p}}{dt} = \frac{1}{2\Psi}[\mathbf{k} - (\mathbf{k}\cdot\mathbf{p})\mathbf{p}] + \frac{1}{2}\boldsymbol{\omega}\times\mathbf{p} + \alpha(\mathbf{I} - \mathbf{pp})\cdot\mathbf{E}\cdot\mathbf{p}, \tag{1}$$

as derived in [23], with factor of two corrected in [24]. Here α is the shape factor which is given for a prolate spheroid as a function of the aspect ratio, n:

$$\alpha = \frac{n^2 - 1}{n^2 + 1}. \tag{2}$$

Many solitary phytoplankton and zooplankton have highly elongated shapes (Fig. 1, b, c). However, some phytoplankton species can also form highly elongated chains via incomplete cell division, such that chains composed of 2, 4, and 8 cells are most routinely observed [25]. Thus, as a single spherical cell forms a chain, its aspect ratio will increase from $n = 1$ ($\alpha = 0$) to $n = 2$ ($\alpha = 0.6$), $n = 4$ ($\alpha \approx 0.88$), and $n = 8$ ($\alpha \approx 0.97$) as it grows in length. In addition, field measurements of cells larger than 2 μm indicate that the overwhelming majority of phytoplankton have elongated morphologies, with $n \approx 5$ being the most frequently observed (though these analyses did not differentiate motile from non-motile species) [26]. In comparison, the non-dimensional parameter Ψ depends on both the properties of the swimmer and flow in which it swims. For example, unicellular phytoplankton swimming in small-scale marine turbulence Ψ is expected to vary between 0.1 to 10 [27], whilst Ψ is expected exceed unity in regions where currents change sharply over the depth of the coastal ocean [15].

We initially consider 2D flow that is either strictly vertical or horizontal, and constrained to the $x - z$ plane, so that $\boldsymbol{\omega} = \omega\mathbf{j}$ and the only non-zero components of $\mathbf{E}$ are $E_{13} = E_{31}$. In section VI we extend this analysis to 3D

flow. It is convenient to consider the cell orientation both in terms of spherical polar angles and in terms of Cartesian co-ordinates:

$$\mathbf{p} = (p_x, p_y, p_z) = (\sin\theta\cos\phi, \sin\theta\sin\phi, \cos\theta), \tag{3}$$

where $\theta \in [0, \pi], \phi \in [0, 2\pi]$.

This yields the following scalar ODEs for spherical polar angles:

$$\frac{d\theta}{dt} = -\frac{1}{2\Psi}\sin\theta + \frac{\omega}{2}\cos\phi + \alpha E_{13}\cos 2\theta\cos\phi, \tag{4}$$

$$\sin\theta\frac{d\phi}{dt} = -\frac{1}{2}(\omega + 2\alpha E_{13})\cos\theta\sin\phi. \tag{5}$$

and for Cartesian co-ordinates:

$$\frac{dp_x}{dt} = \frac{p_z}{2\Psi}\left(-4\alpha E_{13}\Psi p_x^2 - p_x + (\omega + 2\alpha E_{13})\Psi\right), \tag{6}$$

$$\frac{dp_z}{dt} = \frac{1}{2\Psi}\left((-4\alpha E_{13}\Psi p_z^2 - \Psi(\omega - 2\alpha E_{13}))p_x + (1 - p_z^2)\right). \tag{7}$$

The governing equations were integrated using the ode15s solver in MATLAB R2020a using the default values and with a default error tolerance of RelTol=10^{-6}. To improve numerical convergence, at large aspect ratio ($n = 8$) in vertical shear the error tolerance were reduced to AbsTol=10^{-15}, RelTol=10^{-12}, to generate the results shown in figure 4. All code is available from the authors on request.

Furthermore, we make the definition:

$$\sigma = \omega\Psi. \tag{8}$$

For the simple vertical ($\mathbf{u} = -x\mathbf{k}$) and horizontal ($\mathbf{u} = z\mathbf{i}$) shear flows considered in subsequent sections, we have $\omega = 1$ so that σ is identical to Ψ. However, when we consider inhomogeneous Kolmogorov flows, Ψ represents the gyrotactic reorientation timescale normalised by the characteristic vorticity of the flow, and the quantity σ varies in space because it is function of the local vorticity, ω.

III. EQUILIBRIA

P&K found that for vertical shear, $\mathbf{u} = -x\mathbf{k}$, there is only one stable equilibrium, for which $\phi = 0, \cos\theta > 0$ and

$$\sin\theta = \frac{1 - \sqrt{1 - 8\sigma^2\alpha(1-\alpha)}}{4\alpha\sigma}; \tag{9}$$

this exists and is stable if and only if:

$$\sigma < (1+\alpha)^{-1} \quad \text{for} \quad \alpha < 1/3, \quad \text{and} \quad \sigma < (8\alpha(1-\alpha))^{-1/2} \quad \text{for} \quad \alpha > 1/3. \tag{10}$$

For horizontal shear, $\mathbf{u} = z\mathbf{i}$, a stable equilibrium exists only if $\sigma < (1-\alpha)^{-1}$, and has $\phi = 0, \cos\theta > 0$ and

$$\sin\theta = \frac{-1 + \sqrt{1 + 8\sigma^2\alpha(1+\alpha)}}{4\alpha\sigma}. \tag{11}$$

To understand more fully the nature of these equilibria, and in preparation for our explanation of why these point equilibria are not always globally attracting, we first re-derive these results using standard linear stability theory.

For vertical shear, $\mathbf{u} = -x\mathbf{k}$, corresponding to $\omega = 1, E_{13} = -1/2$, equations (4,5,8) yield:

$$\dot{\theta} = \frac{1}{2}g(\theta,\phi) = -\frac{1}{2\sigma}\sin\theta + \frac{1}{2}\cos\phi - \frac{\alpha}{2}\cos 2\theta\cos\phi, \tag{12}$$

$$\sin\theta\dot{\phi} = \frac{1}{2}\sin\theta h(\theta,\phi) = \frac{1}{2}(\alpha - 1)\cos\theta\sin\phi. \tag{13}$$

As P&K, we define the first equilibrium, E1, which lies in the $x - z$ plane:

$$\phi = 0, \quad \sin\theta = \sigma(1 - \alpha\cos 2\theta), \tag{14}$$

and second equilibrium, E2, which lies in the $x-y$ plane, by

$$\theta = \pi/2, \quad \cos\phi = \frac{1}{\sigma(1+\alpha)} \tag{15}$$

which exists only if $\sigma > (1+\alpha)^{-1}$.

Considering E1, on solving equation (14) as a quadratic in $\sin\theta$, we obtain

$$\sin\theta^{\pm} = \frac{1 \pm \sqrt{1-8\sigma^2\alpha(1-\alpha)}}{4\alpha\sigma}. \tag{16}$$

For each equilibrium $\sin\theta^{\pm}$ there are two solutions for θ which we denote θ_{up} (θ_{down}) for $\cos\theta_{up} > 0$ ($\cos\theta_{down} < 0$). To determine the feasibility of the equilibria, we note that E1 equilibria are the roots of $G(\theta) = g(\theta, 0)$ and so by considering the graph of $G(\theta)$, see figure 2, we can determine the number of feasible E1 equilibria (i.e. real and in the domain $\theta \in [0, \pi]$) :

a) Stationary points, $G' = 0$, exist at $\theta = \pi/2$ and $\sin\theta^* = 1/4\alpha\sigma$. For four equilibria to exist, it is necessary for stationary points at θ^* to exist, which requires $\sigma > 1/4\alpha$.

b) For four equilibria to exist, it is necessary that $G(\theta^*) < 0$, which requires $\sigma < (8\alpha(1-\alpha))^{-1/2}$.

c) For four equilibria to exist, it is necessary that $G(\pi/2) > 0$, which requires $\sigma > (1+\alpha)^{-1}$.

d) When only two equilibria exist, it is necessary that $G(\pi/2) < 0$ for the existence of equilibria.

Conditions (a) and (b) cannot simultaneously be satisfied unless $\alpha > 1/3$. Furthermore for $\alpha > 1/3$, condition (c) is more stringent than (a) and so we obtain the result that if $\alpha > 1/3$ there are four distinct equilibria, $\theta^{\pm}_{up}$ and $\theta^{\pm}_{down}$, given by equation (16) (red line in figure 2) provided σ satisfies the following constraint:

$$(1+\alpha)^{-1} < \sigma < (8\alpha(1-\alpha))^{-1/2}. \tag{17}$$

If $\alpha > 1/3$, then there are two distinct equilibria, θ^{-}_{up} and θ^{-}_{down}, (blue line in figure 2) if:

$$0 < \sigma < (1+\alpha)^{-1} \tag{18}$$

given by

$$\sin\theta^{-} = \frac{1 - \sqrt{1-8\sigma^2\alpha(1-\alpha)}}{4\alpha\sigma}, \tag{19}$$

and no equilibria if:

$$(8\alpha(1-\alpha))^{-1/2} < \sigma. \tag{20}$$

If $\alpha < 1/3$ there are two distinct equilibria, θ^{-}_{up} and θ^{-}_{down}, (green line in figure 2) if:

$$0 < \sigma < (1+\alpha)^{-1} \tag{21}$$

also given by equation (19), and no equilibria otherwise (cyan line in figure 2).

By considering $G(\theta)$ we see that in the case where four equilibria exist, two equilibria are stable to perturbations in θ, which are denoted θ^{-}_{up} and θ^{+}_{down}, and two are unstable. In the case where two equilibria exist we have the one stable equilibria, θ^{-}_{up}. However to examine fully the local (linear) stability of the equilibria, including perturbations in ϕ, we need to compute the Jacobian of the system at $E1$, where $\phi = 0$:

$$J = \begin{bmatrix} g_\theta & f_\phi \\ h_\theta & h_\phi \end{bmatrix}_{E1} = \begin{bmatrix} -\frac{1}{\sigma}\cos\theta + 2\alpha\sin 2\theta & 0 \\ 0 & (\alpha-1)\frac{\cos\theta}{\sin\theta} \end{bmatrix}_{E1}. \tag{22}$$

We calculate the determinant of the Jacobian:

$$\mathrm{Det}(J) \;=\; (1-\alpha)\frac{\cos^2\theta}{\sigma\sin\theta}\left(1 - 4\alpha\sigma\sin\theta\right). \tag{23}$$

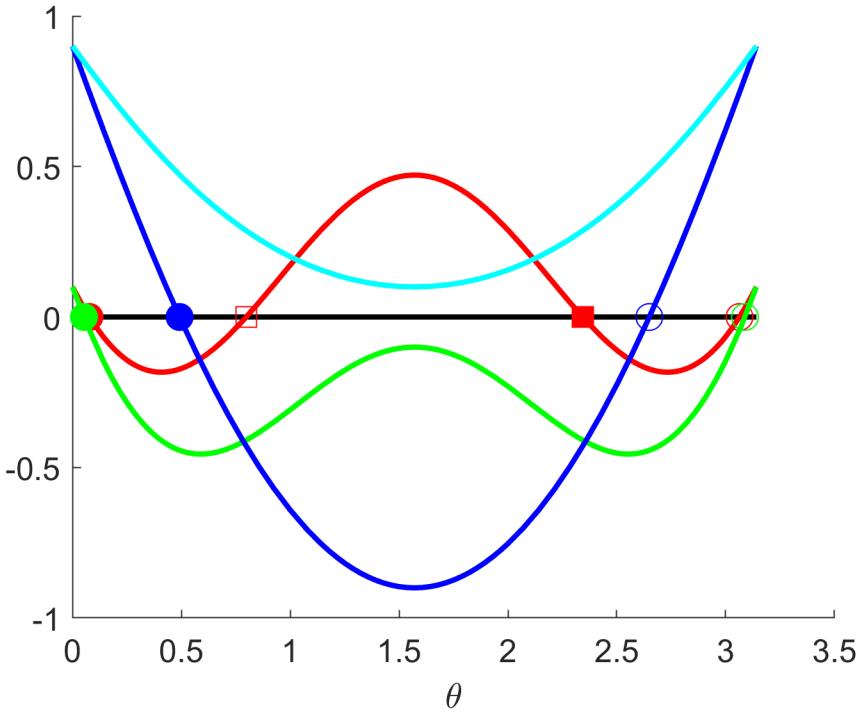

FIG. 2. Function $G(\theta)$ for $\alpha = 0.9, \sigma = 0.7$ (red online, 4 roots, 3 stationary points), $\alpha = 0.9, \sigma = 0.5$ (green online, 2 roots, 3 stationary points), $\alpha = 0.1, \sigma = 0.5$ (blue online, 2 roots, 1 stationary point), $\alpha = 0.1, \sigma = 1$ (cyan online, zero roots, 1 stationary point). Squares are solutions θ^+ and circles θ^-. Filled (empty) symbols indicate (un)stable to small perturbations in θ.

For θ^+, we can substitute the equilibrium solution from equation (16) to obtain:

$$\mathrm{Det}(J) \;=\; -(1-\alpha)\frac{\cos^2\theta}{\sigma\sin\theta}\sqrt{(\cdot)}, \tag{24}$$

where $\sqrt{(\cdot)}$ is the square root appearing in equation (16), and thus we see $\mathrm{Det}(J) < 0$ and hence these equilibria must be unstable. For θ^-, we find $\mathrm{Det}(J) > 0$. We can also compute the trace for θ^-:

$$\mathrm{Trace}(J) \;=\; \frac{\cos\theta}{\sigma\sin\theta}\left(-\sin\theta\sqrt{(\cdot)} - \sigma(1-\alpha)\right). \tag{25}$$

For θ^-_{up}, we find $\mathrm{Trace}(J) < 0$ and $\mathrm{Det}(J) > 0$ hence the equilibrium is stable. Thus we have verified the result obtained by P&K that the only stable equilibria is θ^-_{up} which exists subject to conditions (10).

The second equilibria, E2, is more straightforward. It exists provided $\sigma > (1+\alpha)^{-1}$, with Jacobian that has purely imaginary eigenvalues, hence represented by a circle in the phase plane, and is therefore not linearly stable. We note if $\alpha > 1/3$ then E2 only exists when there are either zero or four E1 equilibria, and when $\alpha < 1/3$, E2 only exists when there are zero E1 equilibria.

The case of horizontal shear is also straightforward. The only change to equation (1) when we change from horizontal to vertical shear is to switch the sign of $\mathbf{E}$, which is equivalent to switching the sign of α. Therefore we can switch the sign of α in equation (16) and subsequent analysis to obtain the equilibria for horizontal shear. In particular, we find that it is not possible to have four E1 equilibria because there are no solutions with $\sin\theta = -1/4\alpha\sigma$ and $\theta \in [0, \pi]$. Furthermore we find that if $\sigma > (1-\alpha)^{-1}$ there is only the E2 equilibrium, and no E1 equilibria. Otherwise, for $\sigma < (1-\alpha)^{-1}$, there are two equilibria given by equation (11), with the up equilibrium being stable and the down equilibrium unstable, and the E2 equilibrium unfeasible.

IV. ORBITS

In figure 3, simulations demonstrate that the point equilibrium is not always globally attracting, and that there exist periodic solutions even when an equilibrium solution is feasible for the given values of parameters α and σ. Such periodic solutions are realised when the initial value of p_x is above a critical value. To understand this more fully it is helpful to consider the nullclines of the dynamical system with respect to p_x and p_z. For vertical shear, $\mathbf{u} = -x\mathbf{k}$, corresponding to $\omega = 1, E_{13} = -1/2$, equations (6,8) yield:

$$\frac{dp_x}{dt} = \frac{p_z}{2\sigma}\left(2\alpha\sigma p_x^2 - p_x + (1-\alpha)\sigma\right), \tag{26}$$

yielding nullclines:

$$p_x^{\pm} = \sin\theta^{\pm} = \frac{1 \pm \sqrt{1 - 8\sigma^2\alpha(1-\alpha)}}{4\alpha\sigma}, \text{ corresponding to } E1, \tag{27}$$

$$p_z = 0, \text{ corresponding to } E2. \tag{28}$$

Similarly, from equation (7), we can obtain:

$$\frac{dp_z}{dt} = \frac{1}{2\sigma}\left((2\alpha\sigma p_z^2 - \sigma(1+\alpha))p_x + (1-p_z^2)\right) = 0 \tag{29}$$

yielding the nullcline:

$$p_x = \frac{p_z^2 - 1}{2\alpha\sigma p_z^2 - \sigma(1+\alpha)}. \tag{30}$$

As discussed in the previous section, when a unique stable equilibrium solution exists, it is in the $x-z$ plane, with $p_x = \sin\theta^-, p_z = \cos\theta^-_{up}$ as indicated by the closed circles in figure 3 and circles in figure 4. The E2 equilibrium corresponds to the point $p_x = (\sigma(1+\alpha))^{-1}, p_z = 0$, as indicated by the closed triangle in figure 3(a).

We see in figure 3a, that if the initial condition satisfies $p_x(0) > \sin\theta^+$, the particle will undergo periodic orbits, clockwise in the $p_x - p_z$ plane, and not be attracted to the stable equilibrium solution. On comparing equations (27) with (16) and subsequent discussion, we see that these periodic orbits will exist provided:

$$(1+\alpha)^{-1} < \sigma < (8\alpha(1-\alpha))^{-1/2}, \tag{31}$$

which we note also requires $\alpha > 1/3$.

By symmetry, for these orbiting trajectories, the mean vertical component is zero. For particles initially distributed uniformly random over the sphere, the ensemble average of the mean vertical component is therefore given by $A\cos\theta^-_{up}$, where $A = \frac{1}{2}(1+\sin\theta^+)$ is the fraction of the surface area of the spherical cap representing the region with initial condition $p_x(0) < \sin\theta^+$. That is, for the parameter region where a stable equilibrium exists but is not globally attracting, the average vertical component of the orientation is given as:

$$\langle p_z \rangle = \frac{1}{2}(1+\sin\theta^+)\cos\theta^-_{up}. \tag{32}$$

This average value is indicated by the open squares in figure 4(b). For the most elongated particles ($n = 8$) we see a slight deviation between the analytical result and that realised through numerical simulations. This occurs because of limitations in the numerical accuracy of the ODE solver which results in some orbiting particles escaping and realising the stable equilibrium. From numerical simulation, we observe that for orbiting trajectories, the mean horizontal component is equal to the value taken at the centre of the orbit, $E2$. For particles initially distributed uniformly random over the sphere, the ensemble average of the mean horizontal component is therefore given as:

$$\langle p_x \rangle = \frac{1}{2}(1+\sin\theta^+)\sin\theta^- + \frac{1}{2\sigma(1+\alpha)}(1-\sin\theta^+), \tag{33}$$

and is indicated by the open squares in figure 4(a).

The governing equations (4,5) are symmetric in ϕ and so we would expect there will be no net transport in the y direction. More specifically, we have shown that the stable equilibrium E1 lies in the $x-z$ plane, and furthermore, for orbiting trajectories, each swimmer with an initial orientation of $p_x(0)$ and mean horizontal component $< p_y >$ will exactly be balanced by a swimmer with an initial orientation of $-p_x(0)$ and mean horizontal component $- < p_y >$. Thus, we would expect that there should be no mean drift of population along y for either cells at a stable equilibrium or those which are orbiting.

For horizontal shear, for $\sigma < (1-\alpha)^{-1}$, there are only two equilibria, and as illustrated in figure 3(b), the up-equilibrium is globally stable. For $\sigma > (1-\alpha)^{-1}$, there are no stable equilibria, and we expect periodic motion.

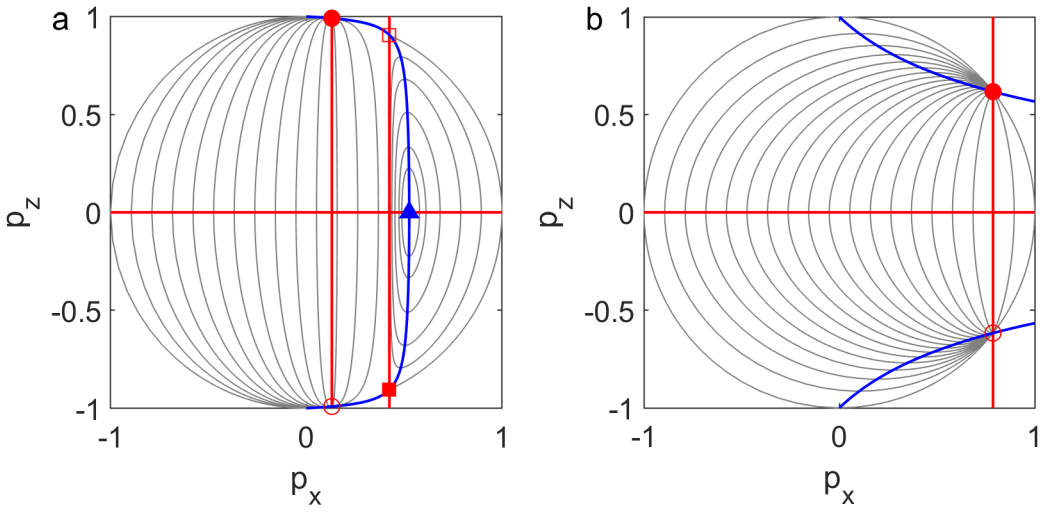

FIG. 3. Phase portrait for horizontal & vertical components of $\mathbf{p}$ with $\alpha = 0.9$ and $\sigma = 1$. Red lines indicate the null-clines $\dot{p}_x = 0$ & blue line is null-cline $\dot{p}_z = 0$. As in figure 2, squares are E1 equilibria θ^+ and circles θ^-. Filled (empty) symbols indicate (un)stable to small perturbations in θ. The E2 equilibrium is indicated by filled blue triangle. (a) Vertical shear, $\mathbf{u} = -x\mathbf{k}$, (b) Horizontal shear, $\mathbf{u} = z\mathbf{i}$.

V. VERTICAL TRANSPORT OF PHYTOPLANKTON

As an illustration of these results, we now consider the deterministic motion of a motile phytoplankton chain n cells in length, which can be modelled as a prolate spheroid with aspect ratio n, centred at position $\mathbf{x}$ with symmetry axis and swimming direction given by the unit vector $\mathbf{p}$ which satisfies the governing equation (1). We suppose the spheroid is advected at the local fluid velocity, $\mathbf{u}$ and swims with velocity $\Phi\mathbf{p}$:

$$\frac{d\mathbf{x}}{dt} = \Phi\mathbf{p} + \mathbf{u}. \tag{34}$$

There are two aspects of vertical transport: (i) the component of upwards swimming, Φp_z; (ii) vertical transport by the flow, u_z. The average upwards swimming component $\Phi\langle p_z\rangle$, displays a non-trivial dependence on chain length, for both simple vertical and horizontal shear flow, as shown in figures 4 & 5. While the upward migration of shorter chains is fully blocked above a critical value of Ψ, longer chains can maintain net upwards motility at larger values of Ψ, indicating that they are better equipped to vertically migrate in strong shear. For $\Psi < 1$ the longest chains have roughly the same upwards migration as observed for spherical swimmers, suggesting that elongation offers neither a significant advantage or disadvantage with shear is relatively weak.

In vertical shear, we also have to consider vertical transport by the flow. To begin, let us consider the parameter space where there exists a globally attracting equilibrium orientation, and consider a swimmer starting from the origin at this equilibrium orientation. In such an idealised scenario, we have that the vertical transport by the flow is given by $u_z = -\Phi p_x t$. In figure 4 we see that an increase in chain length leads to a reduction in the equilibrium value of p_x, reducing the swimmer's downwards advection by the flow and thus enhancing its net upwards transport. More generally, for swimmers not necessarily at equilibrium, a reduction in the average value of the horizontal component of orientation will reduce the downwards advection by the flow, due to u_z linearly decreasing with horizontal position, and thus enhance its net upwards transport.

We also note that for vertical shear, the enhancement of vertical migration conferred by an elongated shape, through an increase in $\langle p_z\rangle$ and a decrease in $\langle p_x\rangle$, can be attenuated relative to that predicted by the equilibrium orientation derived by P&K because the equilibrium solution is not globally attracting for all parameter values. In particular for

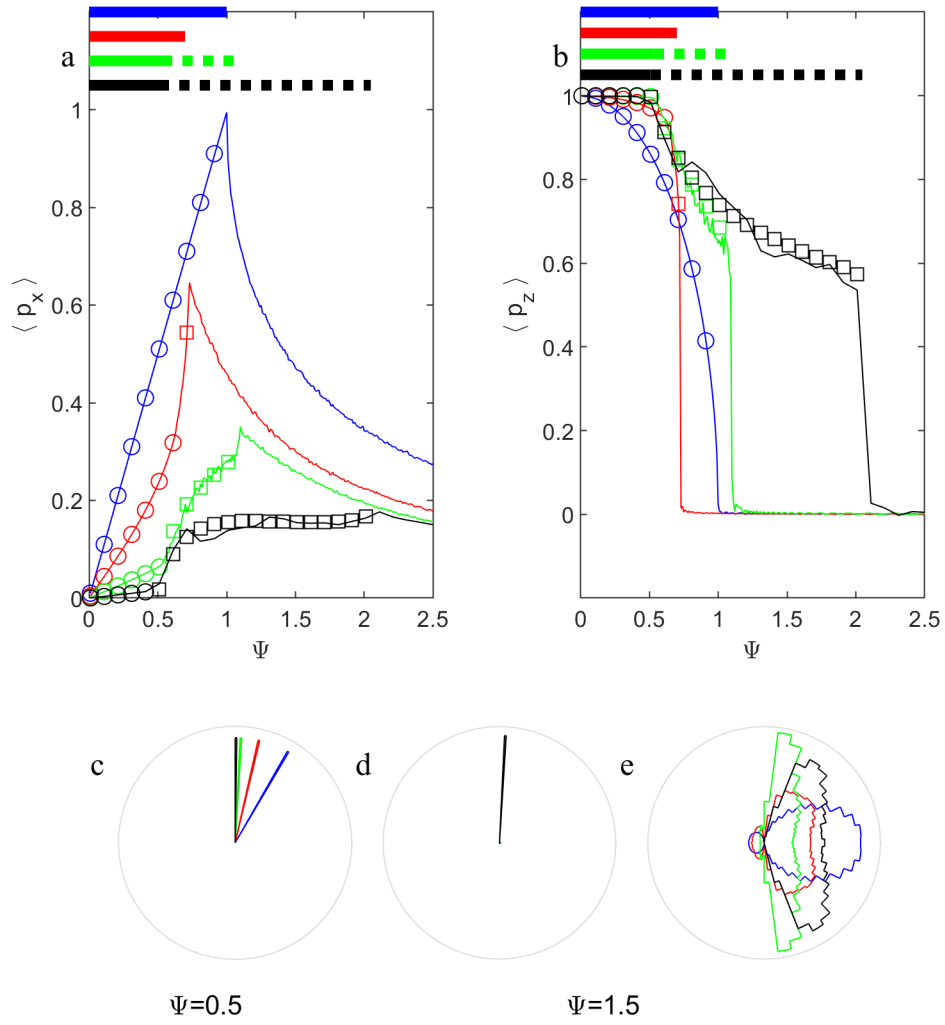

FIG. 4. Orientation in vertical shear, $\mathbf{u} = -x\mathbf{k}$. Horizontal (a) and vertical (b) components of orientation as a function of Ψ for different chain length:$n = 1(\alpha = 0)$, blue; $n = 2(\alpha = 0.6)$, red; $n = 4(\alpha = 0.8824)$, green; $n = 8(\alpha = 0.9692)$, black. The mean (solid line) is computed as the mean of the time-average of each of 1000 trajectories of duration $T = 1000$ starting from random initial orientation uniformly distributed on unit sphere. The thick horizontal bars indicate the range where there exists a stable and globally attracting equilibrium, and circles indicate the stable equilibrium orientation, θ_{up}^{-}. The horizontal dashed lines indicate the range for which the stable equilibrium is not globally attracting, and squares indicate the expected average orientation for this range of Ψ, see equations (32,33). The lower plots show a polar histogram of the orientation distribution for these trajectories projected onto the $x - z$ plane for different chain lengths for $\Psi = 0.5$ (left) and $\Psi = 1.5$ (right). Subplots (c) and (d) are for all trajectories, whereas (e) removes the data points close to the equilibrium orientation to display the distribution of orbiting trajectories.

chains with $n = 4, 8$ we observe in figure 4, for sufficiently large Ψ, the computed average $p_z(p_x)$ value is less (greater) than the equilibrium value for chains of length $n = 4, 8$. We note that in horizontal flow the stable equilibrium is globally attracting when feasible and so the average behaviour is well approximated by the stable equilibrium.

In summary, we can say that spherical swimmers can vertically migrate slightly better than elongated cells for small values of Ψ (in the case of horizontal shear). However, for $\Psi > 1$, elongated swimmers have a major advantage over spherical swimmers, and thus this suggests that elongation enhances vertical migration.

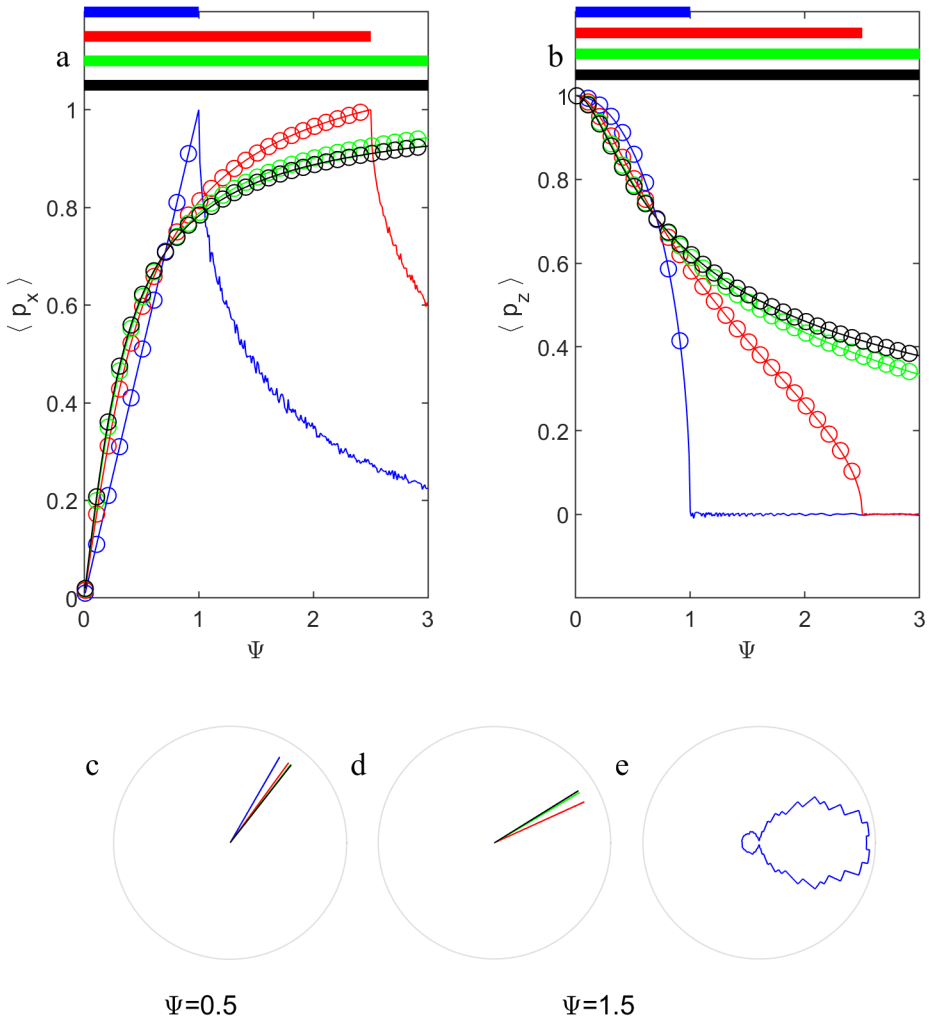

FIG. 5. Orientation in horizontal shear, $\mathbf{u} = z\mathbf{i}$. Horizontal (a) and vertical (b) components of orientation as a function of Ψ for different chain length:$n = 1(\alpha = 0)$, blue; $n = 2(\alpha = 0.6)$, red; $n = 4(\alpha = 0.8824)$, green; $n = 8(\alpha = 0.9692)$, black. The mean (solid line) is computed as the mean of the time-average of each of 100 trajectories of duration $T = 1000$ starting from random initial orientation uniformly distributed on unit sphere, and taking the time-average from $t = 500$ to $t = 1000$, to remove the initial transient behaviour. Circles indicate the stable equilibrium orientation, θ_{up}^{-}, which is always globally attracting when feasible, as indicated by the thick horizontal bars. The lower plots show a polar histogram of the orientation distribution for these trajectories projected onto the $x - z$ plane for different chain lengths for $\Psi = 0.5$ (left) and $\Psi = 1.5$ (right). Subplots (c) and (d) are for all trajectories, whereas (e) removes the data points close to the equilibrium orientation to display the distribution of orbiting trajectories.

A. Kolmogorov flow

We now consider the impact of non-uniform shear on vertical transport and spatial distribution of swimmers using a Kolmogorov flow model within our governing equations for swimmer orientation and position (equations 1 and 34).

1. *Vertical Kolmogorov flow*

We consider the flow field $\mathbf{u} = -\sin(x)\mathbf{k}$, corresponding to $\omega = -\cos(x), E_{13} = -\cos(x)/2$. As shown in figure 6 we see swimmers accumulate in the downwelling region at $x = \pi/2$. The strength of the accumulation increases as

Ψ increases from 0.5 to 1.5. However, as Ψ increases further, swimmers tumble end over end, reducing their overall horizontal migration and consequently the degree to which they accumulate.

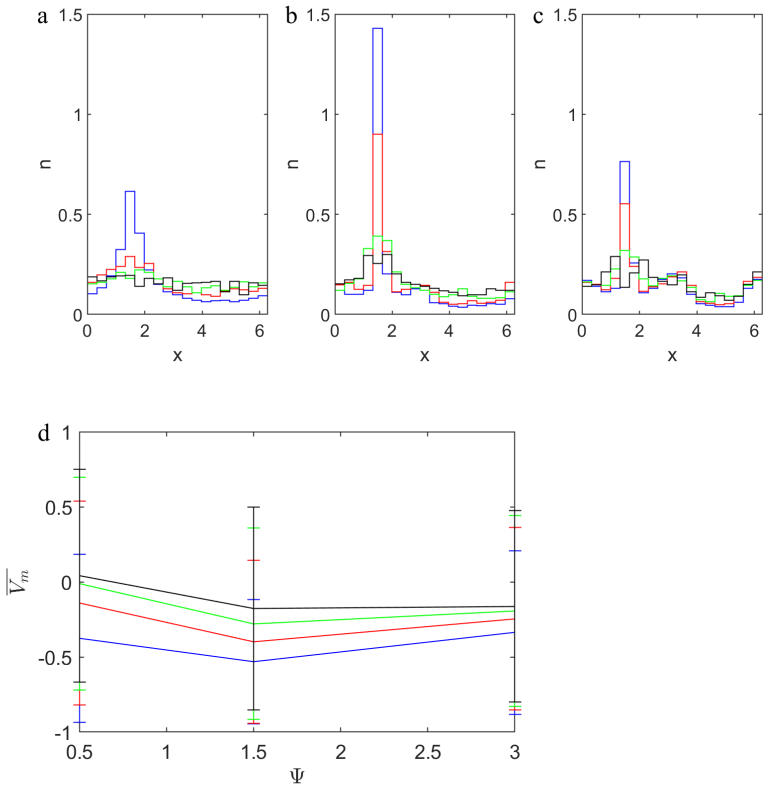

FIG. 6. Swimmers in vertical Kolmogorov flow. (a-c) Histogram of horizontal position (probability distribution, $n(x)$), modulo 2π, over a trajectory for N = 1000 particles of duration $T = 50$ with $\Phi = 0.1$, $\Psi = 0.5(a), 1.5(b), 3(c)$ for different chain length: $n = 1(\alpha = 0)$, blue; $n = 2(\alpha = 0.6)$, red; $n = 4(\alpha = 0.8824)$, green; $n = 8(\alpha = 0.9692)$, black. Particle initial position, x and z, are randomly sampled from $U(0, 2\pi)$, and initial orientation is randomly sampled from unit sphere. The histogram is normalized as a probability density function. (d) The average vertical speed, $\overline{V_m}$, calculated as average vertical displacement of trajectory divided by duration, T, is plotted against Ψ for different chain lengths. Error bars indicate standard deviation.

In figure 6 we also see that elongation decreases the accumulation in the down-welling flow. This can be explained by considering the argument made above describing how elongation reduces the horizontal component of swimming. We thus find that elongation supresses the net downward transport, as illustrated by the increase in the average vertical displacement, see figure 6(d).

2. *Horizontal Kolmogorov flow*

We now consider the flow field $\mathbf{u} = \sin(z)\mathbf{i}$, corresponding to $\omega = \cos(z), E_{13} = \cos(z)/2$. In figure 7, we see the general pattern in spatial distribution corresponds to the phenomenon of gyrotactic trapping with accumulation in high shear regions ($z \approx 0, \pi$) and depletion in low shear ($z \approx \pi/2, 3\pi/2$). At the lower value of stability number ($\Psi = 0.5$), we see a slight enhancement of accumulation in high-shear regions for longer chains, figure 7(a). If the cell orientation is assumed to attain the equilibrium obtained for the local shear, that is the equilibrium discussed in section III, but taking $\sigma = \Psi \cos z$, which is globally attracting for all vertical positions and chain lengths for $\Psi = 0.5$, the conservation equation which describes the evolution of cell density, $n(z, t)$ can be written as:

$$\frac{\partial n}{\partial t} = -\frac{\partial}{\partial z}(\Phi p_z n), \tag{35}$$

which has equilibrium $n_{eq} \propto 1/p_z$, as depicted in figure 7(d). At equilibrium the vertical component of orientation, p_z, decreases monotonically with increasing shear (Figure 5), hence swimmers accumulate in regions of high shear. This behaviour was previously shown for sinking elongated particles in Kolmogorov flow [28]. Furthermore we see that for longer chains, p_z will vary more between the regions of minimum ($\sigma = \Psi \cos z = 0$) and maximum ($\sigma = \Psi \cos z = 0.5$) local shear, hence in Kolmogorov flow, at low values of Ψ, we expect to see higher levels of accumulation for longer chains.

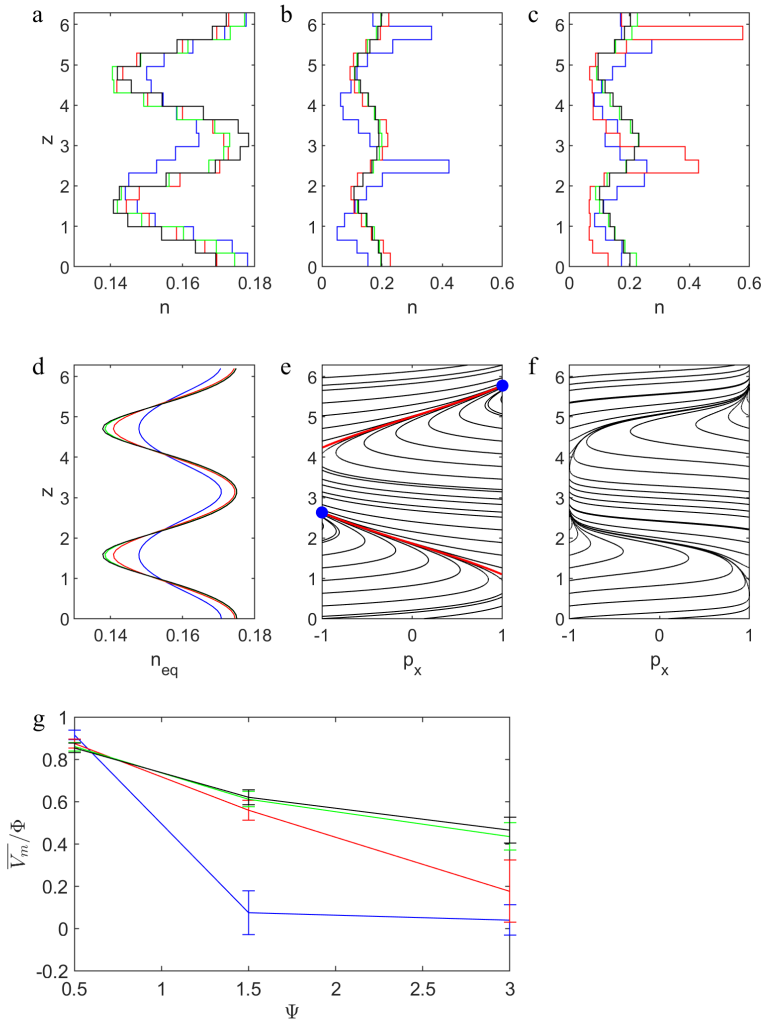

FIG. 7. Swimmers in horizontal Kolmogorov flow. (a-c) Histogram of vertical position (probability distribution, $n(z)$), modulo 2π, over a trajectory for $N = 1000$ particles of duration $T = 50$ with $\Phi = 0.1$, $\Psi = 0.5(a), 1.5(b), 3(c)$ for different chain length: $n = 1$ ($\alpha = 0$), blue; $n = 2$ ($\alpha = 0.6$), red; $n = 4$ ($\alpha = 0.8824$), green; $n = 8$ ($\alpha = 0.9692$), black. Particle initial position, x and z, are randomly sampled from $U(0, 2\pi)$, and initial orientation is randomly sampled from unit sphere. The histogram is normalized as a probability density function. (d) The equilibrium distribution, computed as inversely proportional to the average swimming velocity, p_z, for $\Psi = 0.5$. (e, f) Phase portrait in $p_x - z$ space for (e) $n = 1$ ($\alpha = 0), \Psi = 1.5$ and (f) $n = 2$ ($\alpha = 0.6), \Psi = 3$, indicating how swimmers move upwards and are trapped when they encounter sufficient shear to generate tumbling. Red lines indicate attracting manifold (equation 40), blue circles the transition to tumbling (equation 41). (g) The average vertical speed, $\overline{V_m}$, calculated as average vertical displacement of trajectory divided by duration, T, normalised by swimming speed, Φ, is plotted against Ψ for different chain lengths. Error bars indicate standard deviation.

Additional non-linear effects associated with chain length are apparent at higher values of Ψ where there are tumbling regions. At the intermediate value of stability number ($\Psi = 1.5$), the spheres have the most noticeable peak in

accumulation, figure 7(b), and this exists slightly below the maximum shear regions. This can be explained by considering the vertical component of swimming depicted in figure 5; for $\Psi = 1.5$, whilst there exists a stable equilibrium for upward swimming of chains, spheres undergo tumbles due to a lack of stable equilibrium. In Kolmogorov flow, spherical swimmers swim upwards through the low shear region (where a local equilibrium orientation does exist, $\sigma = \Psi \cos z < 1$), but upon arriving at a vertical position with a higher shear ($\sigma = \Psi \cos z > 1$) they start to tumble. This tumbling behaviour manifests itself as an accumulation of swimmers just below the peak in shear.

To understand this more fully, we note that the key dynamics of the system can be described by the following pair of equations:

$$\frac{dp_x}{dt} = \frac{p_z}{2\Psi}\left(-2\alpha\cos(z)\Psi p_x^2 - p_x + (1+\alpha)\cos(z)\Psi\right), \tag{36}$$

$$\frac{dz}{dt} = \Phi p_z, \tag{37}$$

which, provided $p_z \neq 0$ can be combined to obtain

$$\frac{dp_x}{dz} = \frac{1}{2\Psi\Phi}\left(-2\alpha\cos(z)\Psi p_x^2 - p_x + (1+\alpha)\cos(z)\Psi\right). \tag{38}$$

In the case where $\alpha = 0$, this has solution described by the quantity

$$H(p_x, z) = \Phi \exp\left(\frac{z}{2\Psi\Phi}\right)\left(p_x - \frac{\Psi}{1+4\Psi^2\Phi^2}(\cos z + 2\Psi\Phi\sin z)\right) \tag{39}$$

which is conserved by the dynamics, as previously discussed [16]. By considering this conserved quantity, and from figure 7(e), we see that attracting manifolds, indicated in red in the figure, are defined by the equation

$$p_x = \frac{\Psi}{1+4\Psi^2\Phi^2}(\cos z + 2\Psi\Phi\sin z). \tag{40}$$

The transition to tumbling occurs when $p_x = \pm 1$ on this manifold which is where we see the peak accumulation:

$$z = \arcsin\left(\frac{\sqrt{1+4\Psi^2\Phi^2}}{\Psi}\right) - \arctan\left(\frac{1}{2\Psi\Phi}\right). \tag{41}$$

For the higher value of stability number ($\Psi = 3$) we see the maximum peak is for the slightly elongated swimmers $n = 2(\alpha = 0.6)$, figure 7(c). These parameters yield a sufficient region of vertical space in which swimmers can move upwards, and regions where the shear is sufficiently high for swimmers to tumble and get trapped, as is indicated in the phase portrait shown in figure 7(f).

As a consequence of this trapping behaviour, in figure 7(g) we see that elongation enhances vertical migration. Specifically, we see that the average vertical speed reduces with increasing Ψ, but that elongation suppresses the reduction.

B. Resolving the effect of rotational diffusion

To include rotational diffusion, we first consider the relevant Fokker-Planck equation, from which we can derive the corresponding SDE which can then be used to simulate stochastic trajectories. In a spatially homogeneous system, we take $f(\mathbf{p}, t)$ as the probability of finding a cell with orientation $\mathbf{p}$ at time t to satisfy the Fokker-Planck equation, representing conservation of swimmers [29]:

$$\frac{\partial f}{\partial t} + \nabla \cdot (\mathbf{j}_d + \mathbf{j}_f) = 0, \tag{42}$$

where $\mathbf{j}_d$ and $\mathbf{j}_f$ are the probability current densities due to diffusion and due to the field respectively. For simplicity we assume isotropic diffusion:

$$\mathbf{j}_d = -d_r \nabla f,$$

and in our model for swimmers we have that:

$$\mathbf{j}_f = \dot{\mathbf{p}} f,$$

where $\dot{\mathbf{p}}$ is defined by equation 1, as considered in [23]. This equation can then be written explicitly in terms of the angles θ and ϕ:

$$\frac{\partial f}{\partial t}+\frac{1}{\sin\theta}\left(\frac{\partial}{\partial\theta}\left(\dot{\theta}\sin\theta f\right)+\frac{\partial}{\partial\phi}\left(\dot{\phi}\sin\theta f\right)\right)-d_r\left(\frac{1}{\sin\theta}\frac{\partial}{\partial\theta}\left(\sin\theta\frac{\partial f}{\partial\theta}\right)+\frac{1}{\sin^2\theta}\frac{\partial^2 f}{\partial\phi^2}\right)=0, \tag{43}$$

where $\dot{\theta}$ and $\dot{\phi}$ are defined in equations (4,5). On making the transformation $F=f\sin\theta$ so that $\int F d\theta d\phi=1$, we can write this in the standard form:

$$\frac{\partial F}{\partial t}+\left(\frac{\partial}{\partial\theta}\left(\dot{\theta}F+d_r\cot\theta F\right)+\frac{\partial}{\partial\phi}\left(\dot{\phi}F\right)\right)-d_r\left(\frac{\partial^2 F}{\partial\theta^2}+\frac{1}{\sin^2\theta}\frac{\partial^2 F}{\partial\phi^2}\right)=0, \tag{44}$$

which is equivalent to the following SDE [30]:

$$d\begin{pmatrix}\theta\\ \phi\end{pmatrix}=\begin{pmatrix}\dot{\theta}+d_r\cot\theta\\ \dot{\phi}\end{pmatrix}dt+\sqrt{2d_r}\begin{pmatrix}1 & 0\\ 0 & 1/\sin\theta\end{pmatrix}d\mathbf{W}. \tag{45}$$

We simulate this SDE using the simByEuler solver in MATLAB R2020a with default values and $dt=0.01$. The effect of rotational diffusion on swimmers in horizontal Kolmogorov flow is shown in figure 8. We see rotational diffusion spreads out the peaks in distribution that arise relative to the deterministic case as depicted in figure 7 but elongation still results in enhanced vertical migration for sufficiently small values of rotational diffusion. Specifically, for $d_r=0.01$, we still can see accumulation in layers which is shape dependent, and enhancement of vertical migration due to elongation. We see a reduction in this enhancement as the rotational diffusion is increased to $d_r=0.05$ and $d_r=0.1$.

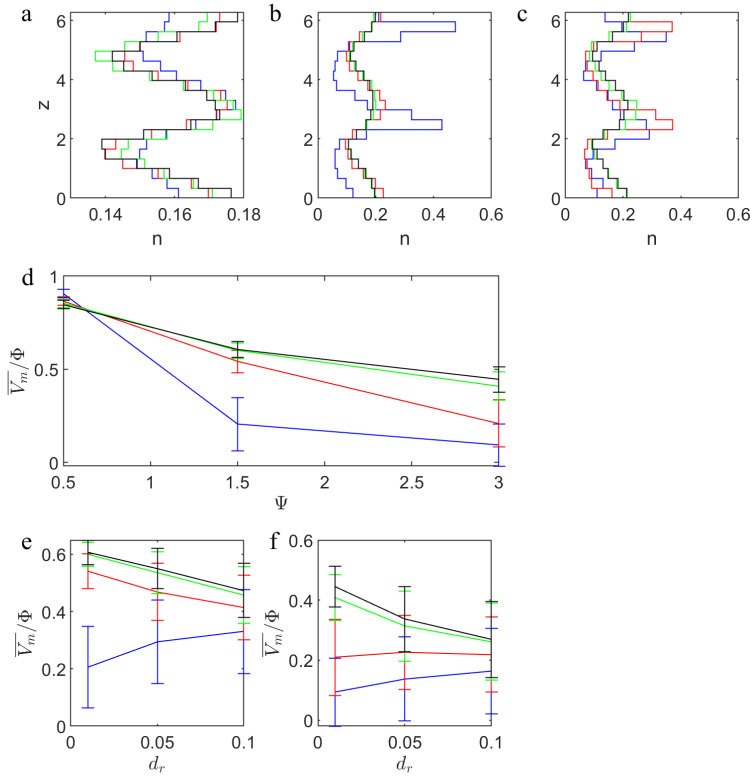

FIG. 8. Swimmers in horizontal Kolmogorov flow with addition of rotational diffusion. (a-c) Histogram of vertical position as figure 7 but with rotational diffusion $d_r=0.01$. The average vertical speed, $\overline{V_m}$, calculated as in figure 7 is plotted as (d) a function of Ψ for fixed $d_r=0.01$ and as a function of d_r for fixed (e) $\Psi=1.5$ and (f) $\Psi=3$.

VI. FLOW WITH NON-ZERO VERTICAL COMPONENT OF VORTICITY

As an investigation of the impact of non-zero vertical component of vorticity, we consider adding $-\epsilon y\mathbf{i}$ to our simple horizontal and vertical shear flows. This yields vorticty $\boldsymbol{\omega} = \omega_2\mathbf{j}+\epsilon\mathbf{k}$, where we introduce the notation ω_2 to represent the y-component of vorticity (denoted by ω in previous sections when the vorticity was purely in the y-direction). We also note that in the rate of strain tensor, the component $E_{12} = -\epsilon/2$, is now non-zero. From equation 1 we can derive scalar ODEs for the spherical polar angles:

$$\frac{d\theta}{dt} = -\frac{1}{2\Psi}\sin\theta + \frac{\omega_2}{2}\cos\phi + \alpha(E_{13}\cos 2\theta + E_{12}\sin 2\theta\sin\phi)\cos\phi, \tag{46}$$

$$\sin\theta\frac{d\phi}{dt} = -\frac{1}{2}(\omega_2 + 2\alpha E_{13})\cos\theta\sin\phi + \frac{1}{2}(\epsilon + 2\alpha E_{12}\cos 2\phi)\sin\theta. \tag{47}$$

We first consider modifying simple vertical shear, $\mathbf{u} = -x\mathbf{k}$; so take $\omega_2 = 1; E_{13} = -1/2$ which yields the perturbed equations:

$$\frac{d\theta}{dt} = -\frac{1}{2\Psi}\sin\theta + \frac{1}{2}\cos\phi - \frac{\alpha}{2}\cos 2\theta\cos\phi - \frac{\alpha\epsilon}{4}\sin 2\theta\sin 2\phi, \tag{48}$$

$$\sin\theta\frac{d\phi}{dt} = \frac{1}{2}(\alpha-1)\cos\theta\sin\phi + \frac{\epsilon}{2}\sin\theta - \frac{\alpha\epsilon}{2}\sin\theta\cos 2\phi. \tag{49}$$

For spherical cells, $\alpha = 0$, we can derive the equilibrium orientation discussed by P&K:

$$0 = -\frac{1}{\Psi}\sin\theta + \cos\phi, \tag{50}$$

$$0 = -\cos\theta\sin\phi + \epsilon\sin\theta, \tag{51}$$

which has a feasible, and stable for the upwards solution, $\cos\theta > 0$, equilibrium:

$$p_z^2 = \cos^2\theta = \frac{1}{2}\left(1 - \Psi^2\omega^2 + \sqrt{(1-\Psi^2\omega^2)^2 + 4\epsilon^2\Psi^2}\right) \tag{52}$$

where $\omega^2 = 1+\epsilon^2$ is the square of total vorticity. We note that this equilibrium is the same as that obtained for spherical cells with $\epsilon = 0$; that is $\sin\theta = \Psi\omega$, but whereas the equilibrium was only feasible for $\Psi\omega < 1$ for spheres, this equilibrium for non-zero ϵ exists for all values of $\Psi\omega$. For elongated shapes ($\alpha > 0$), an analytic expression for the equilibrium is not obvious, but numerical experiments indicate a number of equilibrium states that are distinct from the $\epsilon = 0$ case. In particular, for sufficiently large values of α, at small Ψ we maintain a globally attracting equilibrium; at moderate Ψ, a new locally stable downwards equilibrium coexists with a locally stable upwards equilibrium; and then at larger Ψ the downwards equilibrium co-exists with periodic solutions (Fig. 9).

The impact of these regimes can be seen on the mean vertical component of orientation, (Fig. 10a). For spheres, we see that the effect of this enhanced stability on vertical migration, where the analytic prediction of the equilibrium value of p_z (blue circles) given by equation 52 shows close agreement with the average vertical component of motility, $\langle p_z\rangle$, from the numerical simulations. For elongated cells, for $n = 8(\alpha = 0.9692)$, we see a relatively smooth change in the mean component, $\langle p_z\rangle$, at small values of Ψ, when there exists a globally attracting equilibrium, followed by a noisy, approximately linear drop in the region of Ψ where two equilibria co-exist, followed by a big decrease in the region of Ψ where a stable down-equilibrium co-exists with periodic solutions. Interestingly, the numerical simulations indicate that the mean upwards component of swimming tends to a Ψ-independent value which varies with α. For spheres ($\alpha = 0$), from equations (50-52), the large Ψ equilibrium is given by $\cos\phi = 0, \cos\theta = \epsilon/\omega$. However, the Ψ-independent solution is not a simple equilibrium for all α; for example for $n = 8(\alpha = 0.9692)$, cells attain either a locally-stable down equilibrium or undergo periodic orbits (Fig. 9, g-i) at large values of Ψ .

On considering horizontal shear, $\mathbf{u} = z\mathbf{i}$; we have $\omega_2 = 1; E_{13} = 1/2$ which yields the perturbed equations:

$$\frac{d\theta}{dt} = -\frac{1}{2\Psi}\sin\theta + \frac{1}{2}\cos\phi + \frac{\alpha}{2}\cos 2\theta\cos\phi - \frac{\alpha\epsilon}{4}\sin 2\theta\sin 2\phi, \tag{53}$$

$$\sin\theta\frac{d\phi}{dt} = -\frac{1}{2}(\alpha+1)\cos\theta\sin\phi + \frac{\epsilon}{2}\sin\theta - \frac{\alpha\epsilon}{2}\sin\theta\cos 2\phi. \tag{54}$$

From numerical investigation, we find this system has a globally attracting equilibrium for all values of Ψ. Furthermore, in the limit of large Ψ, this equilibrium is independent of α and given by $\cos\phi = 0, \cos\theta = \epsilon/\omega$. We can see the overall impact of this on the net vertical swimming component in Fig. 10.

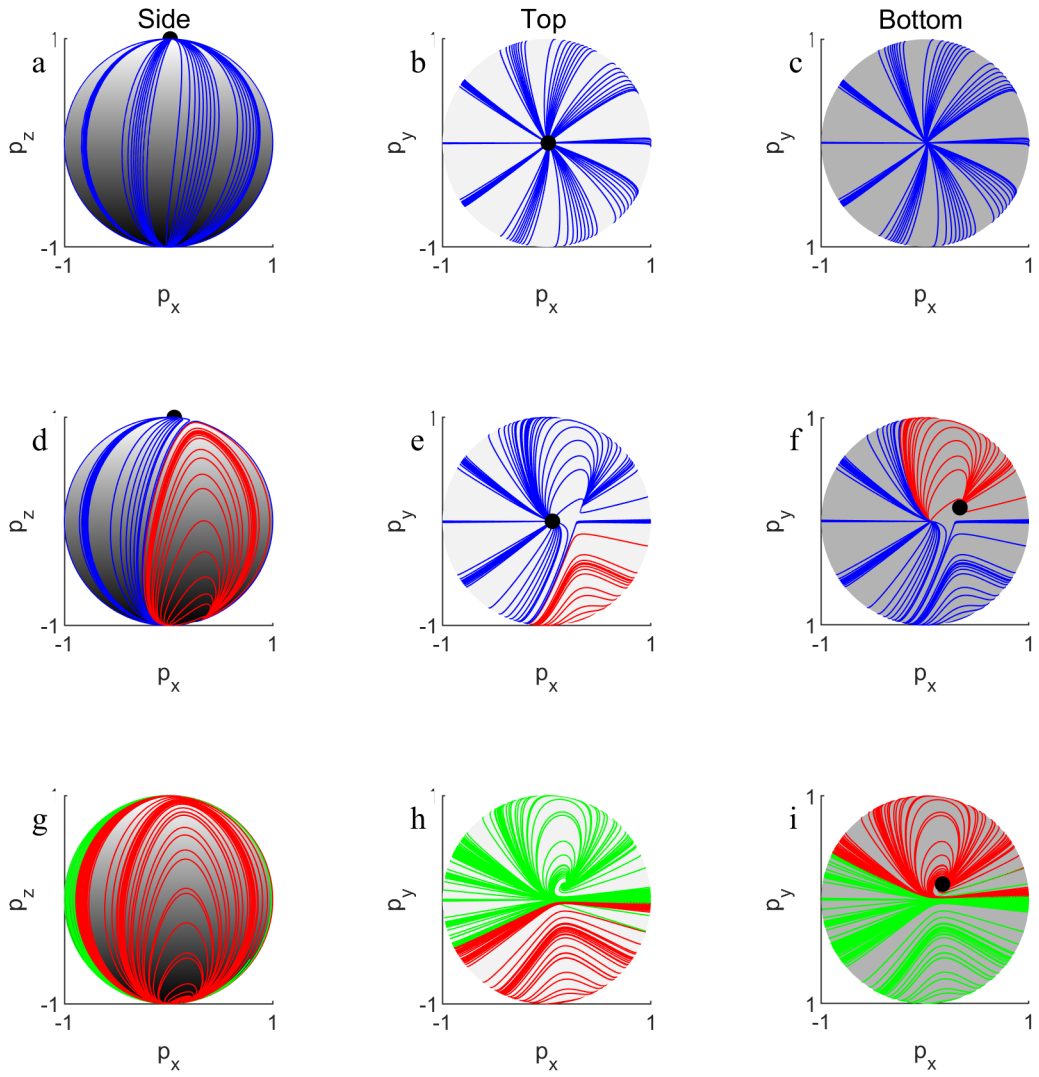

FIG. 9. Phase portrait of $\mathbf{p}$ with $n = 8(\alpha = 0.9692)$ for vertical shear and an additional small component of vertical vorticity $\mathbf{u} = -x\mathbf{k} - \epsilon y\mathbf{i}$, for $\epsilon = 0.1$, as a function of Ψ: (a-c) $\Psi = 0.5$, (d-f) $\Psi = 1.5$, (g-i) $\Psi = 3$. Blue (red) lines indicate trajectories which attain an upwards (downwards) equilibrium orientation and green lines indicate trajectories which do not attain an equilibrium. Black dots indicate the equilibrium orientation.

VII. DISCUSSION

This study uses simple mechanistic models to resolve how the shape of swimmers affects their capacity to migrate through hydrodynamic shear. A swimmer's capacity to vertically migrate depends on two factors: how much of their motility they can direct in the vertical direction (i.e. $\langle p_z \rangle$) and how an organism samples vertical flows in their environment (i.e. $\langle u_z \rangle$). Using a model of simple shear, we demonstrate that elongation can enhance vertical migration via both factors. For certain initial conditions, swimmers can reach a stable equilibrium orientation [13] while for others swimmers undergo a stable limit cycle [14]. When averaged over the full range of possible initial orientations, our results show that spherical swimmers cannot bias their motility in the direction of migration ($\langle p_z \rangle = 0$) whenever $\Psi > 1$ in both horizontal and vertical shear flows, whilst swimmers with elongated morphologies can, on average, still migrate when the stability number increases above unity. In horizontal shear flows the benefit conferred by elongation is substantial when $\Psi > 1$, with $\langle p_z \rangle$ increasing monotonically with swimmer aspect ratio. In a vertical shear flow, the increase in $\langle p_z \rangle$ conferred by an elongated morphology is more modest, benefiting only those that are highly elongated swimmers (e.g. swimmers with $n = 8$ can direct their motility in the vertical direction up until $\Psi \approx 2$). However,

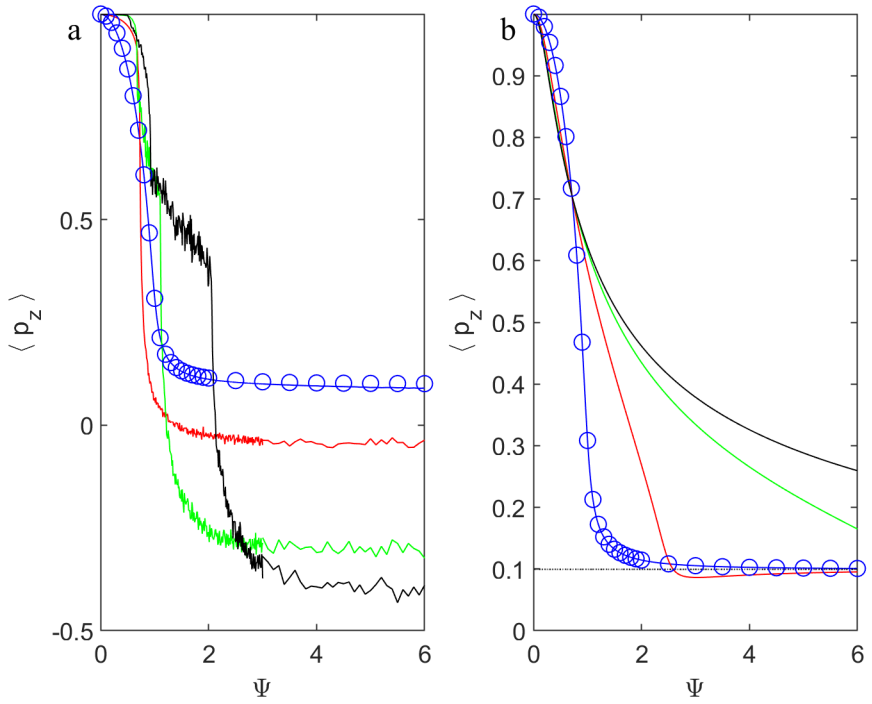

FIG. 10. Vertical component of orientation with small component of vertical vorticity, $\mathbf{u} = -\epsilon y\mathbf{i}$, for $\epsilon = 0.1$, as a function of Ψ for different chain length: $n = 1(\alpha = 0)$, blue; $n = 2(\alpha = 0.6)$, red; $n = 4(\alpha = 0.8824)$, green; $n = 8(\alpha = 0.9692)$, black. (a) Modification of vertical shear $\mathbf{u} = -x\mathbf{k}$, with the mean (solid line) computed as the mean of the time-average of each of 1000 trajectories of duration $T = 1000$ starting from random initial orientation uniformly distributed on unit sphere. Circles indicate the stable equilibrium orientation determined analytically for spheres, $\alpha = 0$. (b) Modification of horizontal shear, $\mathbf{u} = z\mathbf{i}$. The solid lines are the equilibrium orientation attained by cells (note that for spheres this is the same for both the left and right panels). The large Ψ equilibrium orientation, $p_z = \cos\theta = \epsilon/(\sqrt{\epsilon^2 + 1}) \approx 0.995$, which is independent of Ψ and α, is indicated by dotted black line.

in vertical shear flows even slightly elongated morphologies benefit instead from a slower migration in the horizontal direction, which reduces their tendency to swim towards vertical flows that oppose the direction of their migration. Taken together, our analyses using simple shear suggest that elongation enhances vertical migration in the $\Psi > 1$ regime. In the $\Psi < 1$ regime, which corresponds to conditions in which all swimmers can already generally vertically migrate, elongation might offer a slight benefit or a slight detriment to vertical migration.

To explore how these effects play out when the fluid shear varies in space, we next analysed how swimmers with different aspect ratios navigate a sinusoidal Kolmogorov flow in both the vertical and horizontal direction. In vertical flow, it has long been known that gyrotactic organisms that swim upwards tend to accumulate in regions of downwelling [9], impeding cell migration. As predicted by our analyses in simple shear, we find that elongation can enhance vertical migration by preventing swimmers from drifting horizontally to accumulate in downwelling regions (Fig. 6a-c). For this reason, we observe that the overall rate of vertical migration increases monotonically with the aspect ratio of the swimmers (Fig. 6d). Because the vertical flows in aquatic environments can easily exceed the swimming speed of organisms [31], we expect that elongation can enhance vertical migration by preventing swimmers from accumulating in vertical flows that transport them in the direction opposite to that of their migration.

In horizontal Kolmogorov flow, swimmers tend to accumulate in high shear regions. Accumulations are strongest when Ψ is sufficiently large to fully arrest vertical migration via gyrotactic trapping at some depths, but Ψ is sufficiently small to permit vertical migration from a large range of other depths into the trapping regions [16]. We observe the resulting thin layer accumulations depend strongly on swimmer shape, with different aspect ratios forming the strongest accumulations at different values of Ψ. For example, spherical swimmers form the strongest accumulations for $\Psi = 1.5$, whereas swimmers with an aspect ratio of $n = 2$ form the strongest accumulations for $\Psi = 3$. These findings can be rationalised using our results from simple shear, which shows that spherical swimmers become trapped when $\sigma = \omega\Psi$ locally exceeds unity, whereas swimmers with an aspect ratio of two only become trapped once σ locally exceeds 2.5 (Fig. 5). Thus for a Kolmogorov flow with $\Psi = 1.5$, spherical swimmers are gyrotactically trapped in

regions where shear is large, whereas the swimmers with larger aspect ratios are not gyrotactically trapped at any depth (Fig. 5). For $\Psi = 3$, our results from simple shear predict swimmers with $n = 1$ and $n = 2$ both can become gyrotactically trapped. However, swimmers with $n = 2$ form stronger accumulations than spherical swimmers in horizontal Kolmogorov flow because they can swim upwards over larger proportion of the depth, which allows a larger fraction of them to accumulate at the bottom edge of the trapping region. Our findings from horizontal Kolmogorov flow could have implications on the behaviour of vertically migrating populations in the field, where variations in shear routinely occur over depth [7, 32]. Our results suggest such flows could selectively trap swimmers with a particular aspect ratios at particular depth. This flow induced "sorting by aspect ratio" could potentially affect important processes such as predation and viral infection, which are often highly species specific and a strong function of local cell density.

It was recently demonstrated that including the effect of rotational diffusion, which simulates the inherent stochastic variation found in the motility of swimmers, can help spherical swimmers escape thin layer accumulations [16]. However, we find that rotational diffusion does not affect the qualitative trends that we observed for swimmers with different aspect ratios, suggesting that our general conclusions are robust.

We then extended our model of simple shear to resolve how the presence of a weakly three-dimensional flow affects rates of vertical migration. Pedley and Kessler (1987) found that, for spherical swimmers, a nonzero ϵ generates a stable up-swimming equilibrium for all values of ϵ but they did not test whether this equilibrium was globally attracting, nor did they consider non-spherical swimmers in this 3D flow. In the case of spherical swimmers ($\alpha = 0$), our new simulations show that introducing a nonzero ϵ causes the up-swimming equilibrium analytically predicted by Pedley and Kessler (1987) to be globally attracting for all initial conditions for all values of ϵ. In general, spherical swimmers experiencing the weakly three dimensional flow are able to keep a larger fraction of their motility directed in the vertical direction compared to that in a strictly 2D shear flow, i.e. when ϵ is non-zero, $\langle p_z \rangle$ maintains a positive value for larger values of Ψ compared to the $\epsilon = 0$ case (i.e. compare Figs. 4 and 5 to Fig. 10).

For non-spherical particles swimming in a horizontal shear flow, we find that adding a small component of vertical vorticity extends the range of Ψ over which a stable equilibrium exists, and this equilibrium is attained more rapidly for more elongated shapes. Thus, compared to a strictly 2D horizontal shear flow ($\epsilon = 0$), a weakly 3D flow (non-zero ϵ) increases the range of Ψ over which elongation enhances the vertical component of swimming velocity (see Fig. 10b).

For non-spherical particles in a 2D vertical shear flow ($\epsilon = 0$), sufficiently elongated swimmers exhibit three different regimes as Ψ increases: a globally attracting stable upswimming equilibrium; a local upswimming equilibrium combined periodic orbits; all periodic orbits. In vertical shear with non-zero ϵ we find a novel qualitatively different outcome for a vertical shear flow when swimmers are highly elongated. At small Ψ we maintain a globally attracting equilibrium; at moderate Ψ a new locally stable downwards equilibrium coexists with a locally stable upwards equilibrium, and then at larger Ψ , the downwards equilibrium co-exists with periodic solutions (see Fig. 9). For this 3D flow, we again find that elongation enhances the vertical component of swimming velocity (see Fig. 10a); albeit for large values of Ψ and strongly elongated cells, the migration is enhanced in the downwards direction.

Our model of a weakly 3D vertical shear flow suggests that highly elongated cells might switch from swimming up at low shear to swimming down at high shear, unless they are capable of actively modifying their behaviour. Intriguingly, recent experiments found that several species of vertically migrating phytoplankton do actively reverse the direction of their migration in response to flow. [10]. Specifically, it was observed that when a culture of upwards swimming phytoplankton cells undergoes periodic solid body rotation (similar in magnitude to the vorticity they experience in their natural habitat), a fraction of the population switches to a vertically downward migration within minutes [10]. Our model suggests this behavioural switch might actually allow those cells to keep migrating in the same vertical direction as they were before they were exposed to flow i.e. because the behaviourally induced reversal in migration direction would counterbalance the physical mechanism illustrated by our model. Thus, flow-induced change in migration direction observed experimentally might serve as a "bet-hedging" strategy to ensure that a fraction of the population continues migrating in the correct direction. Interestingly, our model of weakly 3D vertical shear flow suggests that elongated cells capable of such a behavioural switch will again migrate faster than spherical cells when Ψ is large (Fig. 10a).

VIII. CONCLUSIONS

Most of what we know about the movement of planktonic organisms comes from benchtop laboratory experiments conducted in quiescent conditions. In their native habitat, however, motile plankton routinely traverse tens of meters of the water column each day, where they must navigate hydrodynamic shear owing to both currents and small-scale turbulence. While novel laboratory techniques [e.g 10, 15, 33], insitu field measurements [e.g. 34, 35], and direct numerical simulations of turbulent flow [e.g. 21, 36] are beginning to provide tools to resolve the behavioural and

physical mechanisms involved in diurnal vertical migrations, conceptual mathematical models are required to both interpret data and test alternative hypotheses. In particular, the interaction between turbulent flow and planktonic organisms often requires abstract models to resolve the underlying physical processes [e.g. 3, 31, 37].

It is has long been understood that the interaction of gyrotactic motility with fluid flow can drive striking accumulations of cells. Numerous studies have investigated how swimmer morphology can affect this clustering process using a wide range of different flow patterns, including Taylor-Green vortex flow [18, 19], Arnold–Beltrami–Childress (ABC) flow [18], bioconvective flows [20, 38] and homogenous, isotropic turbulence [22, 39, 40]. However, the behaviour of swimmers in each these flow models exhibits unique features, making it difficult to generalise the underlying mechanisms. Compared to the comprehensive analyses of clustering, relatively little attention has been paid to how a swimmer's morphology impacts its ability to vertically migrate through flow. A recent study showed that elongated morphologies can enhance the vertical migration of swimmers through a direct numerical simulation (DNS) of turbulence [21], but is it unclear whether this depends on the intricacies of unsteady turbulence or it occurs more widely across a broader range of different flows.

This study illustrates uses models of simple shear to demonstrate how morphology affects a swimmer's ability to migrate through flow. In particular, we investigate two distinct mechanisms that allow elongated swimmers to vertically migrate through shear more rapidly than spherically shaped ones. First, spherical swimmers are widely known to cluster in regions of the flow that moves in a direction opposite to their migration direction [9, 27], such that advection impedes their ability to vertically migrate. However, DNS and statistical models of turbulence have more recently shown that this phenomenon can be reduced or even reversed for swimmers with more elongated morphologies [21, 22, 40]. Our study shows that this behaviour can be recapitulated in a model of simple shear, by demonstrating that elongation inhibits the tendency of swimmers to migrate toward vertical flows that oppose their migration (Fig. 4). Our results therefore indicate that this mechanism does not only occur in turbulence, but rather will be conserved across a wide variety of flows, including Kolmogorov flow (Fig. 6).

A second mechanism that allows elongated swimmers to migrate more rapidly through turbulent flow was recently identified in a direct numerical simulation of homogenous, isotropic turbulence [21]. Elongated swimmers in a direct numerical simulation of turbulence were found to able to keep a larger fraction of their motility pointed in the vertical direction compared to spherical swimmers with the same non-dimensional stability (i.e. elongated swimmers have a larger $\langle p_z \rangle$ compared to spherical swimmers with the same Ψ). However, the physical mechanism that underlies this observation remained unexplained. Our results clearly show that elongated swimmers benefit from a dramatic enhancement in $\langle p_z \rangle$ when $\Psi > 1$ in simple shear (Fig. 4 and 5), again demonstrating this mechanism is not specific to turbulent flow. While here we have assumed, like previous studies, that elongated swimmers behave as prolate spheroids, this study provides a blueprint for how to predict how more complex swimmer body morphologies (e.g. Fig. 1b,c), will affect rates of vertical migration without resorting to methods like DNS of turbulence, where more complicated swimmer morphologies are much more different to represent.

It is widely known that diverse evolutionary pressures contribute to the morphology of motile organisms, including hydrodynamic drag, chemotactic efficiency, collective motility, and construction cost [41–43] . This study resolves the fundamental mechanisms that allow non-spherical swimmers to negotiate hydrodynamic shear, adding to a growing body of evidence that shape plays a pivotal role in an organism's ability perform vertical migrations in the face of the flow that is ubiquitous in aquatic habitats. For simplicity, we assumed in our model that a swimmer's shape can be tuned independently from its swimming speed and stability, however, it is likely an organism's shape will impact both these parameters [21], in addition to the aforementioned processes. We therefore expect the observed shape of swimming organisms has evolved in response to tradeoffs between a number of different factors, including the one investigated here.

It should be noted that in many swimming organisms shape is not necessarily a static trait, but can change in response to external stimuli. For example it has been observed that flow induces swimming phytoplankton to change shape, via either changes in the morphology of single cells [10, 44] or by stimulating the formation of highly elongated chains via incomplete cell division [25]. It therefore appears that vertically migrating swimmers could potentially become more elongated when they need to migrate through vigorous flow, whilst maintaining a more spherical shape at other times to, for example, minimise predation risk [45].

Beyond planktonic organisms, these results may provide new insights to rationally design artificial microswimmers capable of navigating the challenging hydrodynamic conditions often found in engineered systems and the human body (Fig. 1D). The motility of these microswimmers is usually guided via externally applied magnetic fields, which can be modelled using a framework analogous to the mechanism of gravitational reorientation considered here. While we consider relatively simple flows in this study, the methodology used here could be extended to more complex, physiologically relevant flows [46, 47], potentially using approaches from control theory [48] or reinforcement learning [49, 50] to dynamically modulate shape and/or reorientation direction to enhance transport through flow.

In conclusion, the interplay between a swimmer's shape and its ability to navigate through hydrodynamic shear has wide-ranging implications, from understanding how flow impacts the vertical migrations of the plankton that drive

the dynamics of the marine food web to the rational design of microscopic swimmers to deliver therapeutic payloads *in vivo* through vasculature. While the physical mechanisms that underlie interactions between flow and motility are often difficult to resolve in complex flows like turbulence, the simple models described here can recapitulate many of the same phenomena and resolve the underlying mechanistic processes. Such insights offer a new lens through which to interpret how planktonic organisms have adapted to migrate through flow and may ultimately inform the design of bio-inspired microswimmers that can navigate challenging hydrodynamic conditions.

ACKNOWLEDGMENTS

WMD initiated the original idea of investigating the impact of elongation on the vertical transport of microswimmers in simple shear. RNB undertook the mathematical modelling and numerical simulations, with preliminary work carried out with K. Hursthouse as part of an undergraduate project at the University of Liverpool. WMD and RNB jointly wrote the manuscript. We also acknowledge support from the COST Action MP1305: Flowing matter, which facilitated discussions relating to this article during the workshop 'Microorganisms in Turbulent Flows', Lorentz Centre, Leiden, the Netherlands.

[1] G. B. Jeffery, The Motion of Ellipsoidal Particles Immersed in a Viscous Fluid, Proc. Roy. Soc. London Ser. A **102**, 161 (1922).
[2] L. G. Leal and E. J. Hinch, The rheology of a suspension of nearly spherical particles subject to Brownian rotations, J. Fluid Mech. **55**, 745 (1972).
[3] M. N. Ardekani, G. Sardina, L. Brandt, L. Karp-Boss, R. N. Bearon, and E. A. Variano, Sedimentation of inertia-less prolate spheroids in homogenous isotropic turbulence with application to non-motile phytoplankton, J. Fluid Mech. **831**, 655 (2017).
[4] Marcos, J. R. Seymour, M. Luhar, W. M. Durham, J. G. Mitchell, A. Macke, R. Stocker, and J. P. Gollub, Microbial alignment in flow changes ocean light climate, Proc. Nat. Acad. Sci. **108**, 3860 (2017).
[5] G. C. Hays, A review of the adaptive significance and ecosystem consequences of zooplankton diel vertical migrations, Hydrobiologia **503**, 163 (2003).
[6] S. M. Bollens, G. Rollwagen-Bollens, J. A. Quenette, and A. B. Bochdansky, Cascading migrations and implications for vertical fluxes in pelagic ecosystems, Journal of Plankton Research **33**, 349 (2010), https://academic.oup.com/plankt/article-pdf/33/3/349/4203451/fbq152.pdf.
[7] J. P. Ryan, M. A. McManus, and J. M. Sullivan, Interacting physical, chemical and biological forcing of phytoplankton thin-layer variability in Monterey Bay, California, Continental Shelf Research **30**, 7 (2010).
[8] R. Hemmersbach and D.-P. Häder, Graviresponses of certain ciliates and flagellates, The FASEB Journal **13**, S69 (1999), https://faseb.onlinelibrary.wiley.com/doi/pdf/10.1096/fasebj.13.9001.s69.
[9] J. O. Kessler, Hydrodynamic focusing of motile algal cells, Nature **313**, 218 (1985).
[10] A. Sengupta, F. Carrara, and R. Stocker, Phytoplankton can actively diversify their migration strategy in response to turbulent cues, Nature **543**, 555 (2017).
[11] S. O'Malley and M. A. Bees, The orientation of swimming biflagellates in shear flows, Bull. Math. Biol. **74**, 232 (2012).
[12] L. Zhang, J. J. Abbott, L. Dong, B. E. Kratochvil, D. Bell, and B. J. Nelson, Artificial bacterial flagella: Fabrication and magnetic control, Applied Physics Letters **94**, 064107 (2009), https://doi.org/10.1063/1.3079655.
[13] T. J. Pedley and J. O. Kessler, The orientation of spheroidal microorganisms swimming in a flow field, Proc. Roy. Soc. London Ser. B **231**, 47 (1987).
[14] Y. Almog and I. Frankel, The motion of axisymmetric dipolar particles in homogeneous shear flow, J. Fluid Mech. **289**, 243 (1995).
[15] W. M. Durham, J. O. Kessler, and R. Stocker, Disruption of vertical motility by shear triggers formation of thin phytoplankton layers, Science **323**, 1067 (2009).
[16] F. Santamaria, F. De Lillo, M. Cencini, and G. Boffetta, Gyrotactic trapping in laminar and turbulent kolmogorov flow, Phys. Fluids **26**, 111901 (2014).
[17] M. Cencini, G. Boffetta, M. Borgnino, and F. De Lillo, Gyrotactic phytoplankton in laminar and turbulent flows: A dynamical systems approach, Eur. Phys. J. E **42** (2014).
[18] S. I. H. Richardson, N. A. Hill, and A. W. Baggaley, Gyrotactic suppression and emergence of chaotic trajectories of swimming particles in three-dimensional flows, Phys. Rev. Fluids **3** (2017).
[19] W. M. Durham, E. Climent, and R. Stocker, Gyrotaxis in a steady vortical flow, Phys. Rev. Lett. **106**, 238102 (2011).
[20] M. A. Bees, Advances in bioconvection, Annu. Rev. Fluid. Mech. **52**, 449 (2020).
[21] S. Lovecchio, E. Climent, R. Stocker, and W. M. Durham, Chain formation can enhance the vertical migration of phytoplankton through turbulence, Science Advances **5** (2019).
[22] M. Borgnino, G. Boffetta, F. De Lillo, and M. Cencini, Gyrotactic swimmers in turbulence: Shape effects and role of the large-scale flow, J. Fluid Mech. **856**, R11 (2018).

[23] T. J. Pedley and J. O. Kessler, A new continuum model for suspensions of gyrotactic microorganisms, J. Fluid. Mech. **212**, 155 (1990).

[24] T. J. Pedley and J. O. Kessler, Hydrodynamic phenomena in suspensions of swimming microorganisms, Annu. Rev. Fluid. Mech. **24**, 313 (1992).

[25] J. M. Sullivan, E. Swift, P. L. Donaghay, and J. E. Rines, Small-scale turbulence affects the division rate and morphology of two red-tide dinoflagellates, Harmful Algae **2**, 183 (2003).

[26] W. Clavano, E. Boss, and L. Karp-Boss, Inherent optical properties of non-spherical marine-like particles, from theory to observation, Oceanography and marine biology **45**, 1 (2007).

[27] W. M. Durham, E. Climent, M. Barry, F. D. Lillo, G. Boffetta, M. Cencini, and R. Stocker, Turbulence drives microscale patches of motile phytoplankton, Nature Comm. **4**, 2148 (2013).

[28] W. Clifton, R. N. Bearon, and M. A. Bees, Enhanced sedimentation of elongated plankton in simple flows, IMA J. Appl. Math. **83**, 743 (2018).

[29] R. M. Mazo, *Brownian Motion: Fluctuations, Dynamics, and Applications* (Oxford University Press, 2002).

[30] C. Gardiner, *Handbook of Stochastic Methods*, 2nd ed. (Springer-Verlag, 1985).

[31] P. A. Jumars, J. H. Trowbridge, E. Boss, and L. Karp-Boss, Turbulence-plankton interactions: a new cartoon, Marine Ecology **30**, 133 (2009), https://onlinelibrary.wiley.com/doi/pdf/10.1111/j.1439-0485.2009.00288.x.

[32] M. J. Doubell, H. Yamazaki, H. Li, and Y. Kokubu, An advanced laser-based fluorescence microstructure profiler (TurboMAP-L) for measuring bio-physical coupling in aquatic systems, Journal of Plankton Research **31**, 1441 (2009), https://academic.oup.com/plankt/article-pdf/31/12/1441/4335166/fbp092.pdf.

[33] D. Krishnamurthy, H. Li, F. Benoit du Rey, P. Cambournac, A. G. Larson, E. Li, and M. Prakash, Scale-free vertical tracking microscopy, Nature Methods **17**, 1040 (2020).

[34] E. C. Orenstein, D. Ratelle, C. Briseño-Avena, M. L. Carter, P. J. S. Franks, J. S. Jaffe, and P. L. D. Roberts, The scripps plankton camera system: A framework and platform for in situ microscopy, Limnology and Oceanography: Methods **18**, 681 (2020), https://aslopubs.onlinelibrary.wiley.com/doi/pdf/10.1002/lom3.10394.

[35] M. D. Ohman, R. E. Davis, J. T. Sherman, K. R. Grindley, B. M. Whitmore, C. F. Nickels, and J. S. Ellen, Zooglider: An autonomous vehicle for optical and acoustic sensing of zooplankton, Limnology and Oceanography: Methods **17**, 69 (2019), https://aslopubs.onlinelibrary.wiley.com/doi/pdf/10.1002/lom3.10301.

[36] E. Aparicio Medrano, B. van de Wiel, R. Uittenbogaard, L. Dionisio Pires, and H. Clercx, Simulations of the diurnal migration of microcystis aeruginosa based on a scaling model for physical-biological interactions, Ecological Modelling **337**, 200 (2016).

[37] D. M. Lewis, A. Brereton, and J. T. Siddons, A large eddy simulation study of the formation of deep chlorophyll/ biological maxima in un-stratified mixed layers: The roles of turbulent mixing and predation pressure, Limnol. Oceanog. **62**, 2277 (2017).

[38] T. J. Pedley, N. A. Hill, and J. O. Kessler, The growth of bioconvection patterns in a uniform suspension of gyrotactic micro-organisms, Journal of Fluid Mechanics **195**, 223–237 (1988).

[39] C. Zhan, G. Sardina, E. Lushi, and L. Brandt, Accumulation of motile elongated micro-organisms in turbulence, Journal of Fluid Mechanics **739**, 22–36 (2014).

[40] K. Gustavsson, F. Berglund, P. R. Jonsson, and B. Mehlig, Preferential sampling and small-scale clustering of gyrotactic microswimmers in turbulence., Phys. Rev. Lett. **116** (2016).

[41] R. Schuech, T. Hoehfurtner, D. J. Smith, and S. Humphries, Motile curved bacteria are pareto-optimal, Proceedings of the National Academy of Sciences **116**, 14440 (2019), https://www.pnas.org/content/116/29/14440.full.pdf.

[42] O. J. Meacock, A. Doostmohammadi, K. R. Foster, J. M. Yeomans, and W. M. Durham, Bacteria solve the problem of crowding by moving slowly, Nature Physics **17**, 205 (2021).

[43] Ò. Guadayol, K. L. Thornton, and S. Humphries, Cell morphology governs directional control in swimming bacteria, Scientific Reports **7**, 2061 (2017).

[44] M. J. Zirbel, F. Veron, and M. I. Latz, The reversible effect of flow on the morphology of ceratocorys horrida (peridiniales, dinophyta)*, Journal of Phycology **36**, 46 (2000), https://onlinelibrary.wiley.com/doi/pdf/10.1046/j.1529-8817.2000.98088.x.

[45] E. Selander, H. H. Jakobsen, F. Lombard, and T. Kiørboe, Grazer cues induce stealth behavior in marine dinoflagellates, Proceedings of the National Academy of Sciences **108**, 4030 (2011), https://www.pnas.org/content/108/10/4030.full.pdf.

[46] A. Zöttl and H. Stark, Nonlinear Dynamics of a Microswimmer in Poiseuille Flow, Phys. Rev. Lett. **108**, 218104 (2012).

[47] S. A. Berman, J. Buggeln, D. A. Brantley, K. A. Mitchell, and T. H. Solomon, Transport barriers to self-propelled particles in fluid flows, Phys. Rev. Fluids **6**, L012501 (2021).

[48] K. Belharet, D. Folio, and A. Ferreira, Simulation and planning of a magnetically actuated microrobot navigating in the arteries., IEEE Transactions on Biomedical Engineering, Biomedical Engineering, IEEE Transactions on, IEEE Trans. Biomed. Eng **60**, 994 (2013).

[49] S. Colabrese, K. Gustavsson, A. Celani, and L. Biferale, Flow navigation by smart microswimmers via reinforcement learning, Phys. Rev. Lett. **118**, 158004 (2017).

[50] K. Gustavsson, L. Biferale, A. Celani, and S. Colabrese, Finding efficient swimming strategies in a three-dimensional chaotic flow by reinforcement learning, The European Physical Journal E **40**, 110 (2017).